Deep Neural Networks for Precise Brain Tumor Delineation: A U-Net and TensorFlow Approach

Niranjan C. Kundur
Department of Computer Science and Engineering, JSS Academy of Technical Education, Bengaluru, India
niranjanckundur@jssateb.ac.in

H. R. Divakar
Department of MCA, P E S College of Engineering, Mandya, India
divakarhr@gmail.com (corresponding author)

Samitha Khaiyum
Department of MCA, Dayananda Sagar College of Engineering, Bengaluru, India
samitha-mcavtu@dayanandasagar.edu

Kiran P. Rakshitha
Department of MCA, Dayananda Sagar College of Engineering, Bengaluru, India
rakshitha-mcavtu@dayanandasagar.edu

Praveen M. Dhulavvagol
School of Computer Science and Engineering, KLE Technological University, Hubli, India
praveen.md@kletech.ac.in

Anand S. Meti
School of Computer Science and Engineering, KLE Technological University, Hubli, India
anandsmeti@kletech.ac.in

Received: 22 February 2025 | Revised: 20 March 2025 and 7 April 2025 | Accepted: 12 April 2025

 DOI: https://doi.org/10.48084/etasr.10684

ABSTRACT

Brain tumors, especially gliomas, are complex and aggressive growths of cells in the brain that lead to high morbidity and mortality. With high-grade gliomas having a median survival rate of under two years, accurate and timely diagnosis is crucial. Magnetic Resonance Imaging (MRI) is the primary method for detecting brain tumors, but manual interpretation by radiologists can be time-consuming and subject to variability. Therefore, there is a growing need for more reliable and automated methods. This study proposes a deep learning approach for Brain Tumor Segmentation (BraTS) using the U-Net model in TensorFlow. U-Net is well-suited for biomedical image segmentation due to its encoder-decoder structure and skip connections, which capture detailed information and spatial context. The model is trained on the BraTS 2020 dataset, which includes MRI scans of high-grade and low-grade gliomas across four sequences: Fluid-Attenuated Inversion Recovery (FLAIR), T1-weighted, T1-weighted with Contrast Enhancement (T1CE), and T2-weighted. This work demonstrates the potential of deep learning to improve medical imaging precision, enhancing diagnosis and treatment planning for brain tumor patients.

Keywords-brain tumor segmentation; gliomas; deep learning; U-net architecture

I. INTRODUCTION

Brain tumors, particularly gliomas, represent a significant health challenge due to their complexity and potential life-threatening consequences. Gliomas, which affect the Central Nervous System (CNS), are associated with poor prognoses, with high-grade gliomas exhibiting a median survival time of less than two years. The accurate detection and segmentation of brain tumors are crucial for effective diagnosis and treatment planning. MRI is the most common imaging technique used to detect abnormal brain tumors, providing detailed images of brain structures and abnormalities. Traditionally, the analysis of MRI has been performed manually by radiologists, a process that is both time-consuming and prone to inter- and intra-observer variability. Early automated methods for BraTS predominantly utilized handcrafted features and classical machine learning algorithms, such as Support Vector Machines (SVM) and Random Forests. These techniques used features, like intensity, texture, and edge information from MRI scans to classify tumor regions. However, their reliance on manually engineered features limited their ability to fully capture the complex and heterogeneous nature of brain tumors [1, 2]. The implementation of deep learning, particularly Convolutional Neural Networks (CNNs), revolutionized the field of medical image analysis, including BraTS, because of their ability to learn hierarchical feature representations directly from the data, significantly improving segmentation accuracy. Early CNN-based approaches, such as 2D CNNs for slice-wise tumor segmentation, showed promise but were limited by their inability to leverage the full 3D context of MRI volumes [3]. Thus, 3D CNNs were introduced, enabling the model to leverage volumetric data and capture spatial dependencies across different slices of MRI scans.

One of the most prominent architectures in this category is the U-Net. U-Net's encoder-decoder structure, combined with skip connections, allows for the preservation of spatial context while capturing fine details, making it highly effective for tasks, like BraTS [4-7]. Subsequent research has explored various enhancements to the U-Net architecture, including the integration of attention mechanisms, multi-scale feature extraction, and the incorporation of domain-specific knowledge. For instance, the attention U-Net focuses on the most relevant regions of an image, improving segmentation accuracy, particularly for small or diffuse tumor regions [8–10]. Ensemble models combining multiple U-Net variants have also been developed to boost robustness and generalization [11–13]. In addition to architectural advancements, the availability of large, annotated datasets, such as the BraTS challenges, has driven progress in the field by providing a diverse collection of multi-modal MRI scans that serve as standardized benchmarks, facilitating the development of state-of-the-art segmentation methods, many of which are based on variations of the U-Net architecture [14-17]. Despite these advancements, challenges remain in achieving consistent and accurate segmentation across different MRI modalities and patient populations. Variability in image acquisition protocols, tumor morphology, and the presence of imaging artifacts can all affect the performance of automated segmentation methods. As such, ongoing research continues to explore ways to enhance the robustness and generalization of these models, including the use of domain adaptation techniques, synthetic data augmentation, and advanced loss functions tailored for imbalanced datasets [18-20].

This paper proposes an advanced deep learning method for BraTS based on the U-Net architecture, implemented in TensorFlow. The proposed approach leverages the BraTS 2020 dataset [3, 21–23], comprising multi-modal MRI scans FLAIR, T1-weighted, T1CE, and T2-weighted from patients with gliomas, to train and validate the proposed model. The U-Net is designed to segment brain tumors into distinct sub-regions, including edema, non-enhancing tumor core, and enhancing tumor regions. Red-Green-Blue (RGB) color mapping is employed to visually distinguish different tumor subtypes, aiding in the clinical interpretation of segmented images.

II. MATERIALS AND METHODS

Figure 1 illustrates a comprehensive workflow for BraTS using the U-Net architecture. The process begins with an input MRI brain scan, which undergoes a series of data transformation steps to enhance its quality and suitability for analysis. Following preprocessing, the data are partitioned into training, validation, and testing subsets to facilitate model development and evaluation. Subsequently, brain images are sliced to focus on specific regions of interest, narrowing the scope to object regions where tumors are likely to be located. This targeted focus reduces complexity and enhances segmentation precision. The watershed algorithm is applied to segment the regions, particularly useful for separating overlapping areas. Feature scaling is then applied to normalize the data, ensuring that all features contribute equally to the segmentation task, thereby preventing any bias.

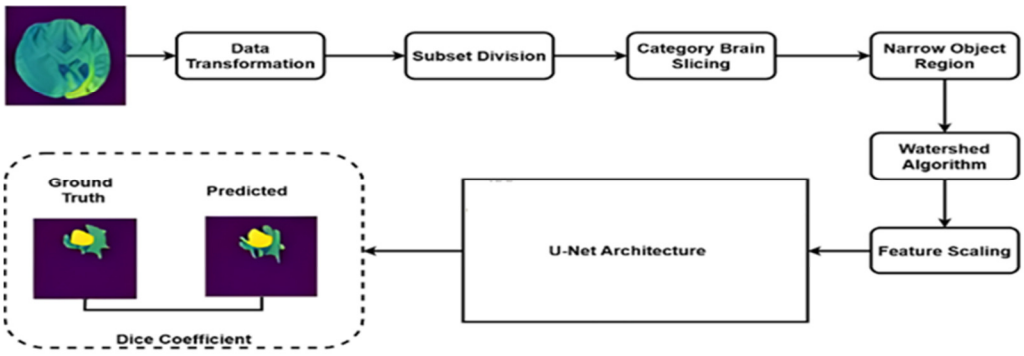

Fig. 1. Proposed system architecture.

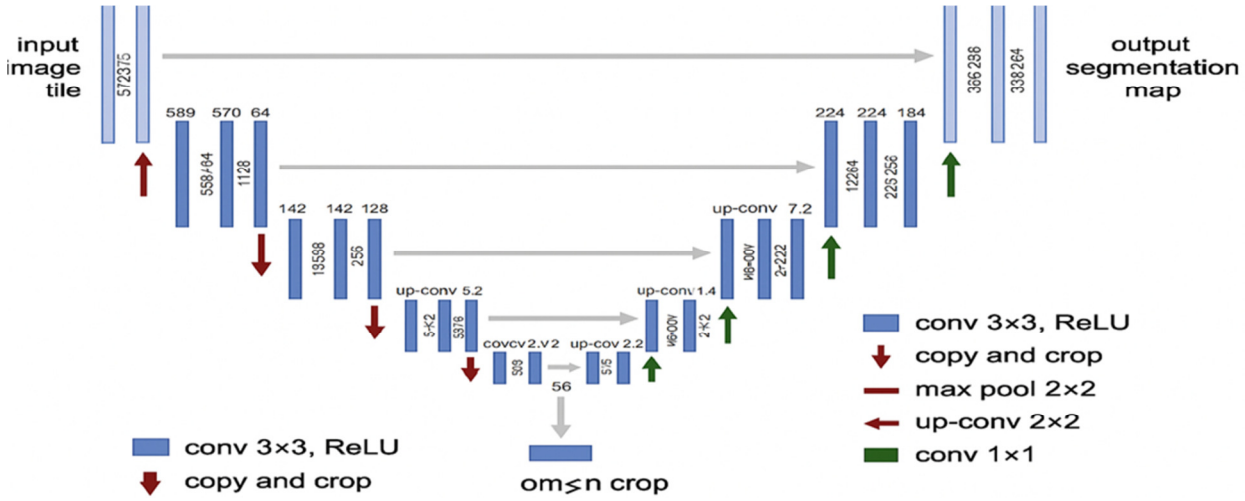

Fig. 2. U-net architecture..

The processed data are then input into the U-Net model, which performs the segmentation task. The model outputs segmented images identifying different tumor sub-regions. These predicted segmentations are evaluated against ground truth annotations using the Dice Coefficient, a widely employed metric that quantifies the overlap between the predicted and actual tumor regions. This metric provides a robust assessment of segmentation accuracy.

A. U-Net Model Architecture

Figure 2 depicts the architecture of a U-Net model. The U-Net features a symmetric encoder-decoder structure, forming a characteristic "U" shape. On the left side, the encoding path (contracting path) begins with the input image of dimensions 64×64×3, where the first two dimensions represent the spatial resolution (height and width) and the third dimension represents the number of channels (features). As data progress through this path, feature maps double in number (64, 128, 256, 512, 1024) while spatial dimensions halve due to 2×2 max pooling operations, capturing increasingly complex features at reduced resolutions. At the base of the U-Net, the network reaches its bottleneck, where the deepest, most abstract feature representations are learned using the highest number of filters (1024). From this point, the decoder (expanding) path mirrors the encoder, but in reverse. Through 2×2 up-sampling operations, the network gradually reconstructs the spatial dimensions of the input, simultaneously halving the number of feature maps (1024, 512, 256, 128, 64) while recovering image resolution. At each up-sampling step, the corresponding high-resolution feature maps from the encoding path are concatenated, allowing the model to leverage both global context and fine-grained details. Following each concatenation, the network applies a series of 3×3 convolutional layers, ReLU activation functions, and batch normalization, further refining the feature maps. The final layer in the decoder uses a 1×1 convolution to reduce the feature map to the number of output classes, which in this case is one, corresponding to the segmented tumor mask. This results in a binary mask output (192, 64, 64, 1) that indicates the presence of a tumor in each pixel of the input image. This architectural design makes the U-Net highly effective for tasks requiring precise localization and segmentation, leveraging both low-level and high-level feature representations throughout its layers.

B. Brain Magnetic Resonance Imaging Segmentation

Figure 3 shows a series of MRI brain scans using different imaging modalities, each contributing unique information for effective BraTS, along with the corresponding segmented output. From left to right, the images display T1-weighted, T1CE, T2-weighted, and FLAIR scans, followed by the final segmentation mask.

The T1-weighted scan offers a high-resolution anatomical baseline, where fat appears bright and water appears dark, providing detailed structural information but limited information regarding sensitivity to pathological changes. The T1CE scan incorporates a contrast agent, which enhances the visualization of abnormal areas by making tumors appear brighter, highlighting regions with disrupted blood-brain barriers. The T2-weighted scan emphasizes regions with high water content, such as edema or cysts, making this modality effective for identifying the extent of abnormal tissue growth and fluid accumulation around tumors. The FLAIR scan specializes in suppressing the bright signal from cerebrospinal fluid, enhancing the visibility of lesions near fluid-filled spaces by displaying pathological tissue in a bright contrast against a dark background. The fourth image in the second row shows the segmentation mask, which is the output of a segmentation model. This mask delineates the tumor region by highlighting it in white against a green background, effectively separating the tumor from surrounding healthy brain tissue.

C. Model Training

The U-Net model is trained on the BraTS 2020 dataset [3, 21-23]. The Adam optimizer is used for optimization. The initial learning rate is set to 1×10^{-4}, and a learning rate scheduler is employed to reduce the learning rate by a factor of 0.1 if the validation loss does not improve for five consecutive epochs. This adaptive learning rate strategy facilitates better convergence to an optimal minimum. To mitigate overfitting, a common challenge when working with limited datasets, regularization techniques such as data augmentation and early

stopping are incorporated, ensuring that the model generalizes well to unseen data.

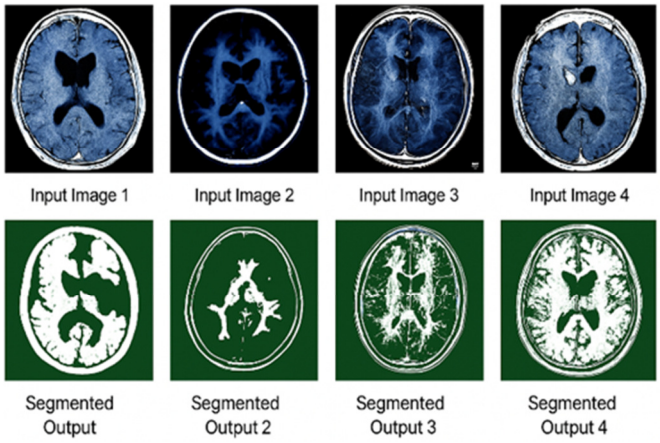

Fig. 3. MRI brain scans using different imaging modalities.

D. Dataset Composition

The BraTS 2020 dataset consists of 369 MRI samples, with each patient's imaging volume encompassing four distinct modalities: T1-weighted, T1CE, T2-weighted, and FLAIR. Each MRI volume is stored as a 3D array with dimensions of 240 x 240 x 155, corresponding to the sagittal, coronal, and axial planes, respectively. This multi-dimensional representation facilitates comprehensive analysis across different anatomical views of the brain.

E. Dataset Preparation

For reliable model performance, the BraTS 2020 dataset is split into three distinct subsets:

- Training Set (259 MRIs, 70%): Used to train the model, allowing it to learn by adjusting its parameters to minimize the error between predicted segmentation masks and ground truth labels.
- Validation Set (55 MRIs, 15%): Utilized during model development to fine-tune hyperparameters, ensuring the selection of the most effective configuration for model optimization.
- Test Set (55 MRIs, 15%): Employed post-training to evaluate the model's performance on unseen data, providing an assessment of its generalization capability.

III. RESULTS AND DISCUSSION

The model was evaluated on the test dataset, and the performance metrics were recorded to assess the effectiveness of the segmentation. The key evaluation metrics include accuracy, Intersection over Union (IoU), dice coefficient, precision, sensitivity, and specificity, and are displayed in Table I. Additionally, a confusion matrix was generated to visualize the performance of the segmentation model in classifying tumor versus non-tumor regions, as can be seen in Figure 4.

TABLE I. PERFORMANCE METRICS OF THE PROPOSED MODEL ON THE TEST DATASET

Metric	Accuracy	IoU	Dice coefficient	Precision	Sensitivity	Specificity
Model performance	89.5%	0.75	0.78	0.81	0.74	0.92

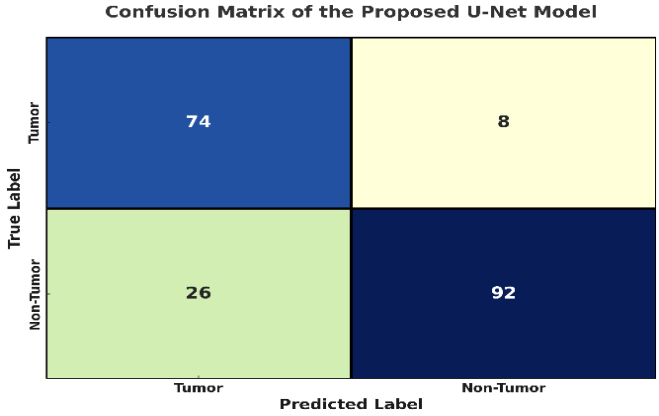

Fig. 4. Confusion matrix for tumor classification.

The confusion matrix illustrates the model's performance in classifying tumor and non-tumor regions. The high true positive (74) and true negative (92) values indicate that the U-Net model accurately detects tumor areas while effectively minimizing false detections, demonstrating strong segmentation reliability.

A. Comparative Study

To evaluate the performance of the proposed model, it was compared with several baseline methods and state-of-the-art techniques. The comparison was based on the same test dataset and evaluation metrics. The compared methods include:

- Baseline Model 1 (Baseline FCN-8s): A traditional segmentation method using thresholding.
- Baseline Model 2 (SegNet): A classical machine learning approach employing SVM.
- State-of-the-Art Model (DeepLabv3): A recent deep learning approach deploying a U-Net architecture optimized for medical imaging.

TABLE II. COMPARATIVE ANALYSIS OF DIFFERENT SEGMENTATION METHODS

Method	Accuracy	IoU	Dice coef.	Precision	Sensi.	Spec.
Baseline FCN-8s [24]	82.3%	0.65	0.67	0.72	0.62	0.88
SegNet [25]	85.4%	0.70	0.72	0.76	0.68	0.90
DeepLabv3 [26]	88.7%	0.74	0.76	0.79	0.71	0.91
U-Net (proposed)	89.5%	0.75	0.78	0.81	0.74	0.92

The results in Table II demonstrate that the proposed model outperforms the baseline methods and is competitive with the state-of-the-art techniques. Specifically, the proposed model achieved the highest overall accuracy and dice coefficient. Several factors contribute to the model's enhanced performance.

- Modalities Selection: The use of T1CE and FLAIR modalities provided complementary information that improved the segmentation accuracy.
- Effective Preprocessing: Techniques, such as normalization and resizing, ensured that the input data were of high quality, facilitating better model training.
- Post-processing Techniques: The application of morphological operations and connected component analysis refined the segmentation results by reducing noise and false positives.

While the model shows promising results, there are areas for further improvement. Future work may include exploring additional modalities, advanced architecture, or integrating ensemble methods to further enhance segmentation performance. Additionally, incorporating larger and more diverse datasets could improve the model's generalizability and robustness.

B. Comparative Analysis

To provide a comprehensive view of the U-Net model's performance, its results were compared with other state-of-the-art segmentation models on similar datasets, listed in Table III. The comparative analysis indicates that the U-Net model slightly outperforms the performance of other models across all metrics, particularly in terms of precision and specificity. This suggests that the U-Net model is highly effective for BraTS, providing valuable insights for clinical use.

TABLE III. COMPARATIVE PERFORMANCE OF THE U-NET MODEL WITH OTHER STATE-OF-THE-ART SEGMENTATION MODELS

Model	Loss	Accuracy	Mean IoU	Dice coefficient	Precision	Sensitivity	Specificity
U-Net (this study)	0.0206	0.9935	0.8176	0.6008	0.9938	0.9922	0.9979
DeepLabv3+ [26]	0.0280	0.9920	0.8050	0.5850	0.9900	0.9800	0.9970
Attention U-Net [27]	0.0254	0.9910	0.8000	0.5800	0.9900	0.9800	0.9950
ResUNet++ [28]	0.0302	0.9895	0.8100	0.5900	0.9850	0.9700	0.9960

IV. CONCLUSION

this study evaluated the performance of a proposed U-Net model for Brain Tumor Segmentation (BraTS), trained on Magnetic Resonance Imaging (MRI) scans from the BRaTS 2020 dataset.

The U-Net model has demonstrated exceptional performance in segmenting brain tumors from MRI images by effectively capturing intricate details while preserving the broader context. The model achieved a low test loss of 0.0206, a Dice Coefficient of 0.6008, a precision of 0.9938, a sensitivity of 0.9922, and a specificity of 0.9979. These metrics not only reflect the model's high accuracy, but also its excellent generalization capabilities when applied to unseen data.

Qualitative assessments further validate the model's proficiency, showing consistent distinction between tumor and non-tumor regions across a range of scenarios, including variations in tumor size and location. This ability underscores the U-Net model's robustness and its potential to significantly enhance diagnostic accuracy. A comparative analysis with other state-of-the-art segmentation models on similar datasets revealed that the proposed model displayed the best metrics among them.

Overall, the current study's findings position the U-Net architecture as a critical tool for clinicians, offering enhanced diagnostic precision and supporting more personalized treatment planning.

REFERENCES

[1] V. P. B. Grover, J. M. Tognarelli, M. M. E. Crossey, I. J. Cox, S. D. Taylor-Robinson, and M. J. W. McPhail, "Magnetic Resonance Imaging: Principles and Techniques: Lessons for Clinicians," *Journal of Clinical and Experimental Hepatology*, vol. 5, no. 3, pp. 246–255, Sep. 2015, https://doi.org/10.1016/j.jceh.2015.08.001.

[2] N. Mo, L. Yan, R. Zhu, and H. Xie, "Class-Specific Anchor Based and Context-Guided Multi-Class Object Detection in High Resolution Remote Sensing Imagery with a Convolutional Neural Network," *Remote Sensing*, vol. 11, no. 3, Jan. 2019, Art. no. 272, https://doi.org/10.3390/rs11030272.

[3] Perelman School of Medicine, University of Pennsylvania. BraTS 2020 Dataset. [Online]. Available: https://www.med.upenn.edu/cbica/brats2020/data.html.

[4] S. Wang and Y. Zhang, "DenseNet-201-Based Deep Neural Network with Composite Learning Factor and Precomputation for Multiple Sclerosis Classification," *ACM Transactions on Multimedia Computing, Communications, and Applications*, vol. 16, no. 2s, pp. 1–19, Apr. 2020, https://doi.org/10.1145/3341095.

[5] R. H. Mwawado, B. J. Maiseli, and M. A. Dida, "Robust Edge Detection Method for Segmentation of Diabetic Foot Ulcer Images," *Engineering, Technology & Applied Science Research*, vol. 10, no. 4, pp. 6034–6040, Aug. 2020, https://doi.org/10.48084/etasr.3495.

[6] S. Albawi, T. A. Mohammed, and S. Al-Zawi, "Understanding of a convolutional neural network," in *2017 International Conference on Engineering and Technology (ICET)*, Antalya, Aug. 2017, pp. 1–6, https://doi.org/10.1109/ICEngTechnol.2017.8308186.

[7] N. C. Kundur, B. C. Anil, P. M. Dhulavvagol, R. Ganiger, and B. Ramadoss, "Pneumonia Detection in Chest X-Rays using Transfer Learning and TPUs," *Engineering, Technology & Applied Science Research*, vol. 13, no. 5, pp. 11878–11883, Oct. 2023, https://doi.org/10.48084/etasr.6335.

[8] P. Roy, S. Dutta, N. Dey, G. Dey, S. Chakraborty, and R. Ray, "Adaptive thresholding: A comparative study," in *2014 International Conference on Control, Instrumentation, Communication and Computational Technologies (ICCICCT)*, Kanyakumari District, India, Jul. 2014, pp. 1182–1186, https://doi.org/10.1109/ICCICCT.2014.6993140.

[9] L. Maurya, V. Lohchab, P. Kumar Mahapatra, and J. Abonyi, "Contrast and brightness balance in image enhancement using Cuckoo Search-optimized image fusion," *Journal of King Saud University - Computer and Information Sciences*, vol. 34, no. 9, pp. 7247–7258, Oct. 2022, https://doi.org/10.1016/j.jksuci.2021.07.008.

[10] G. Maragatham and S. Mansoor Roomi, "A Review of Image Contrast Enhancement Methods and Techniques," *Research Journal of Applied Sciences, Engineering and Technology*, vol. 9, no. 5, pp. 309–326, Feb. 2015, https://doi.org/10.19026/rjaset.9.1409.

[11] A. Patel, "Benign vs Malignant Tumors," *JAMA Oncology*, vol. 6, no. 9, Sep. 2020, Art. no. 1488, https://doi.org/10.1001/jamaoncol.2020.2592.

[12] M. J. McAuliffe, F. M. Lalonde, D. McGarry, W. Gandler, K. Csaky, and B. L. Trus, "Medical Image Processing, Analysis and Visualization in clinical research," in *Proceedings 14th IEEE Symposium on*

Computer-Based Medical Systems. CBMS 2001, Bethesda, MD, USA, 2001, pp. 381–386, https://doi.org/10.1109/CBMS.2001.941749.

[13] W. Rawat and Z. Wang, "Deep Convolutional Neural Networks for Image Classification: A Comprehensive Review," *Neural Computation*, vol. 29, no. 9, pp. 2352–2449, Sep. 2017, https://doi.org/10.1162/neco_a_00990.

[14] S. Thalagala and C. Walgampaya, "Application of AlexNet convolutional neural network architecture-based transfer learning for automated recognition of casting surface defects," in *2021 International Research Conference on Smart Computing and Systems Engineering (SCSE)*, Colombo, Sri Lanka, Sep. 2021, pp. 129–136, https://doi.org/10.1109/SCSE53661.2021.9568315.

[15] O. Ronneberger, P. Fischer, and T. Brox, "U-Net: Convolutional Networks for Biomedical Image Segmentation." arXiv, 2015, https://doi.org/10.48550/ARXIV.1505.04597.

[16] A. El Boustani, M. Aatila, E. El Bachari, and A. El Oirrak, "MRI Brain Images Classification Using Convolutional Neural Networks," in *Advanced Intelligent Systems for Sustainable Development (AI2SD'2019)*, Cham, 2020, vol. 1105, pp. 308–320, https://doi.org/10.1007/978-3-030-36674-2_32.

[17] W. S. Salem, A. F. Seddik, and H. F. Ali, "A Review on Brain MRI Image Segmentation," in *The Second International Conference on New Paradigms in Electronics and Information Technologies PEIT'013*, Luxor, Egypt, Nov. 2013, vol. 1.

[18] Y. Qi et al., "A Comprehensive Overview of Image Enhancement Techniques," Archives of Computational Methods in Engineering, vol. 29, no. 1, pp. 583–607, Jan. 2022, https://doi.org/10.1007/s11831-021-09587-6.

[19] J. Thirumaran and S. Shylaja, "Medical Image Processing-An Introduction," *Computer Graphics and Image Processing*, vol. 4, no. 11, pp. 1197–1199, Nov. 2014.

[20] N. C. Kundur and P. B. Mallikarjuna, "Deep Convolutional Neural Network Architecture for Plant Seedling Classification," *Engineering, Technology & Applied Science Research*, vol. 12, no. 6, pp. 9464–9470, Dec. 2022, https://doi.org/10.48084/etasr.5282.

[21] B. H. Menze *et al.*, "The Multimodal Brain Tumor Image Segmentation Benchmark (BRATS)," *IEEE Transactions on Medical Imaging*, vol. 34, no. 10, pp. 1993–2024, Oct. 2015, https://doi.org/10.1109/TMI.2014.2377694.

[22] S. Bakas *et al.*, "Advancing The Cancer Genome Atlas glioma MRI collections with expert segmentation labels and radiomic features," *Scientific Data*, vol. 4, no. 1, Sep. 2017, Art. no. 170117, https://doi.org/10.1038/sdata.2017.117.

[23] S. Bakas *et al.*, "Identifying the Best Machine Learning Algorithms for Brain Tumor Segmentation, Progression Assessment, and Overall Survival Prediction in the BRATS Challenge." arXiv, Apr. 23, 2019, https://doi.org/10.48550/arXiv.1811.02629.

[24] M. Goyal, P. Rajpura, H. Bojinov, and R. Hegde, "Dataset Augmentation with Synthetic Images Improves Semantic Segmentation," in *Computer Vision, Pattern Recognition, Image Processing, and Graphics*, Singapore, 2018, vol. 841, pp. 348–359, https://doi.org/10.1007/978-981-13-0020-2_31.

[25] V. Badrinarayanan, A. Kendall, and R. Cipolla, "SegNet: A Deep Convolutional Encoder-Decoder Architecture for Image Segmentation," *IEEE Transactions on Pattern Analysis and Machine Intelligence*, vol. 39, no. 12, pp. 2481–2495, Dec. 2017, https://doi.org/10.1109/TPAMI.2016.2644615.

[26] F. Ketenci Çay, Ç. Yeşil, O. Çay, B. G. Yılmaz, F. H. Özçini, and D. İlgüy, "DeepLabv3 + method for detecting and segmenting apical lesions on panoramic radiography," *Clinical Oral Investigations*, vol. 29, no. 2, Jan. 2025, Art. no. 101, https://doi.org/10.1007/s00784-025-06156-0.

[27] O. Oktay *et al.*, "Attention U-Net: Learning Where to Look for the Pancreas." arXiv, May 20, 2018, https://doi.org/10.48550/arXiv.1804.03999.

[28] D. Jha *et al.*, "ResUNet++: An Advanced Architecture for Medical Image Segmentation." arXiv, 2019, https://doi.org/10.48550/ARXIV.1911.07067.